Allele-specific editing of rhodopsin P23H knock-in mice broadens therapeutic potential of CRISPR/Cas for dominant genetic diseases

Short title: CRISPR/Cas9 allele-specific editing for treating dominant genetic diseases

Pingjuan Li[1], Benjamin P. Kleinstiver[2,3,4], Mihoko Y. Leon[1], Michelle S. Prew[2,3], Daniel Navarro-Gomez[1], Scott H. Greenwald[1], Eric A. Pierce[1], J. Keith Joung[2,3,4], Qin Liu[*1]

[1]Ocular Genomics Institute, Massachusetts Eye & Ear, Harvard Medical School, Boston, Massachusetts 02114; [2]Molecular Pathology Unit & Center for Cancer Research, Massachusetts General Hospital, Charlestown, Massachusetts 02129; [3]Center for Computational and Integrative Biology, Massachusetts General Hospital, Boston, Massachusetts 02114; [4]Department of Pathology, Harvard Medical School, Boston, Massachusetts 02114

*Correspondence should be addressed to Q.L.: Qin_Liu@meei.harvard.edu

Abstract

No effective treatment exists for dominant inherited diseases. Here, we present a CRISPR/Cas9 genome editing strategy that combines multiple innovations to achieve specific and efficient disruption of the pathogenic allele with a single-nucleotide mutation (*Rho*-P23H) in a mouse model of dominant retinitis pigmentosa. Our study demonstrates the possibility of a spacer-mediated allele-specific editing approach, which may be applicable to a broad range of dominant disorders in which the mutant allele is not discriminable by placement of a PAM sequence.

Conventional gene augmentation therapies have shown great promise in clinical trials for treating recessive diseases, such as inherited retinal degenerations (IRDs) and hemophilia[1,2]. However, its application to dominant diseases is limited due to the requirement for silencing or ablating the gain-of-function or dominant-negative mutant alleles. While alternative RNA-based suppression-replacement approaches have also been actively pursued, the allelic specificity, longevity of the therapy, and regulation of gene expression levels have posed significant challenges for their broad application[3]. CRISPR/Cas9 gene editing technologies present an alternative approach to treat dominant diseases by addressing these challenges.

The CRISPR/Cas9 system has been revolutionary for genome editing because the Cas9 nuclease can be programmed to generate double-strand DNA breaks at specified genomic sites using a single guide RNA (sgRNA), which dictates much of the target site specificity[4]. The Cas9/sgRNA complex scans the genome for the presence of a protospacer adjacent motif (PAM), the critical first step of DNA target site recognition[4]. Recent studies in mice have shown that, when the disease-causing allele harbors unique PAM sequences that are not present in its wild-type counterpart, allele-specific genome editing by selectively targeting and permanently inactivating the mutant allele could be achieved while leaving the wild-type allele functionally intact[5-7]. However, many dominant alleles do not carry sequences that overlap with a target site PAM, making them refractory to this type of allele-specific editing strategy. One potential approach to expand the applicability of allele-specific genome editing is to develop strategies in which the disease-causing allele can be discriminated from the wild-type allele when the sequence differences are instead positioned within the spacer region of the Cas9/sgRNA target site. Streptococcus pyogenes Cas9 (SpCas9) is known to be generally ineffective at distinguishing between single nucleotide mismatches in much of its spacer sequence[8-10], however, recent studies in human iPSCs and rat embryos have provided some encouraging evidence for the use of mismatches in the spacer sequence to achieve allele-specific genome editing[11-13], suggesting that this strategy might work in a site-dependent manner. Furthermore, recently developed improvements in SpCas9 specificity may be leveraged to improve targeting specificity[14,15]. In the present study, we investigated the feasibility of using this spacer-mediated allele-specific editing to ablate a dominant allele in a *Rhodopsin*-P23H knockin mice. This mouse model genetically and phenotypically recapitulates *rhodopsin*-associated autosomal dominant retinitis pigmentosa (adRP)[16], the most common form of inherited retinal disease[17].

Because the endogenous sequence surrounding the *Rhodopsin*-P23H mutation does not harbor any canonical NGG PAM sites for wild-type SpCas9, we designed two sgRNAs (sgRNA1 and sgRNA2) against sites with non-canonical NNCAGT and NGA PAMs that are accessible for engineered SaCas9-KKH and SpCas9-VQR nucleases, respectively[18,19] (**Fig. 1a**). The position of P23H mutation is 12bp upstream of the PAM in sgRNA1 and 4bp in sgRNA2. Plasmids encoding

the sgRNA and its corresponding Cas9 nuclease were co-delivered via subretinal injection to neonatal mice (P0-P2), followed by *in vivo* electroporation. Assessment of the targeting fficiency and allele-specificity by targeted deep sequencing revealed robust disruption efficiency, but neither nuclease was able to distinguish the mutant P23H allele from the wild-type *Rho* allele, even though both preferentially targeted the mutant allele in heterozygous mice (**Fig. 1b, 1c)**. We therefore examined whether truncated sgRNAs bearing shortened 5' ends, which showed increased specificity of SpCas9 in a previous study[20], could improve allele discrimination. A 17-nucleotide version of sgRNA2 (tru-sgRNA2) was designed and tested. When paired with tru-sgRNA2, SpCas9-VQR exclusively edited the P23H mutant allele with a cleavage efficiency of 28% in the homozygous mutant retinas, and no detectable cleavage in the wild-type controls (**Fig. 1d**). To potentially further improve the on-target editing efficiency, tru-sgRNA2 was paired with SpCas9-VRQR (an improved version of SpCas9-VQR that has enhanced activity; Kleinstiver and Joung, unpublished data) and tested **(Fig. 1e**). The on-target editing frequency induced by SpCas9-VRQR (44.8 ± 4.8%) for the P23H allele was significantly higher relative to SpCas9-VQR (22.1 ± 8.1%, $p<0.001$) in homozygous mice, with a low level of nuclease-induced editing of the wild-type allele (1.3 ± 0.3%) in the wild-type mice. As detailed below, this concomitant targeting of the wild-type allele did not abrogate the observed therapeutic benefit. Off-target cleavage of SpCas9-VRQR/tru-sgRNA2 at other closely matched sites was predicted by CCTop-CRISPR/Cas9 predictor[21]. Evaluation of the top 10 sites by PCR and deep sequencing showed that no indel was detected at 9 sites; while 3.12 ± 2.28% (n=3) of indels was detected at the site in *Gm27760*, which has 1bp mismatch from on-target site sequence (**Supplementary Fig. 1 and Supplementary Table 1, 2**).

To assess the potential therapeutic effectiveness of P23H targeting with SpCas9-VRQR and tru-sgRNA2, we analyzed the insertion or deletion mutation (indel) profiles of edited alleles across 10 independent experimental replicates and observed that 89.5 ± 3.3% of indels created frame shifts (**Fig. 1f, 1g, Supplementary Fig 2**). Moreover, consistent with a previous report [22], the indel pattern is nonrandom; the top two most frequent indels observed across different replicates accounts for 50.2 ± 4.7% of all indels (**Fig. 1h, 1i**). Since the P23H mutation is located in the first exon of *RHO*, frame-shift indels are expected to create null alleles.

To confirm that allele-specific editing leads to altered expression of the mutant allele, we performed RT-PCR followed by targeted deep sequencing to determine the relative mRNA levels of wild-type, P23H and edited alleles in P14 heterozygous retinas. While approximately 22.8% edited alleles were detected at DNA level in the treated retinas (**Fig. 2a**), only 4.8% mRNA from edited alleles were detected, with the majority of them being in-frame (**Fig. 2b**). The ratio of wild-type mRNA (75.5 ± 2.3%) vs mutant P23H and edited mRNA (26.5 ± 2.3%) was significantly increased in the treated cells (2.8 ± 0.35) compared to that in the control cells

(1.37±0.05) (**Fig. 2b, 2c)**. When the mRNA level was normalized to the wild-type allele, the ratio of wt vs. mutant mRNA was 1: 0.35 in the treated cells compared to 1: 0.73 in the untreated cell (**Fig. 2d**), suggesting 38% decrease of mutant mRNA level in the treated cells. This result indicates that 38% of transfected cells express only wild-type rhodopsin, while the transcripts from edited mutant alleles have undergone nonsense mediated decay (**Fig. 2e)**; this is consistent with the finding at the DNA level, where the majority of edited alleles harbor an out-of-frame indel.

To gauge whether ablation of the P23H allele in the treated cells could lead to prevention or delay of photoreceptor degeneration in the regions of retina transfected with SpCas9-VRQR/ tru-sgRNA2 plasmids, we analyzed retinal structure in heterozygous *Rho*-P23H mice 5 weeks post-injection. The photoreceptor outer nuclear layer (ONL) was significantly thicker ($p<0.05$) in the treated EGFP positive region (41.13 ± 4.46 µm) than the adjacent untreated EGFP negative area (23.98 ± 2.39 µm) **(Fig. 2f)**. While five to six rows of photoreceptor cells remained in the treated area, only three to four rows were left in the untreated area **(Fig. 2g)**. Consistent with this finding, immunofluorescence analysis showed that the rhodopsin protein was localized correctly in the outer segments of the transfected photoreceptor cells, consistent with the ablation of the P23H mutant RNA, while in contrast the mutant Rho-P23H protein was mislocalized to the inner segments and cell bodies of the untreated cells **(Fig. 2g)**.

This study demonstrates for the first time that a spacer-mediated allele-specific genome editing approach is feasible to selectively inactivate a missense dominant allele at its native locus. This was accomplished by using a tru-sgRNA along with an alternative SpCas9 variant designed to target an alternative PAM sequence. Using this strategy, we observed a significant decrease of the mutant transcript and protein, which in turn led to preservation of photoreceptor morphology and viability in a mouse model of dominant RP. Similar phenotypic rescue was observed in two previous studies in transgenic mice in which CRISPR/Cas9 ablated the mutant rhodopsin transgene by targeting the sequences that differed between the species and host [23,24]. With the continuing expansion of the CRISPR/Cas nuclease toolbox, many more human dominant alleles may become targetable using a similar allele-specific editing approach. Extending the allele-specific editing beyond discrimination at only the PAM significantly broadens the application of genome editing technologies and could lead to greater number of therapeutics for various dominant genetic diseases. Additional investigations are warranted for advancing this allele-specific approach towards clinical translation, including comprehensive evaluation of off-target activities, the development of more effective *in vivo* delivery, and the valuation of long-term therapeutic benefits and safety.

Online Methods.

Mouse Husbandry. Our study conforms to the Association for Research in Vision and Ophthalmology Statement for the Use of Animals in Ophthalmic and Vision Research. All procedures were approved by the Animal Care and Use Committees of the Schepens Eye Research Institute. *Rho*-P23H mouse line were purchased from the Jackson Lab (stock No. 017628) and maintained in the animal facility at Schepens Eye Research Institute on a 12h: 12h light/dark circle. F1 heterozygous progeny of P23H homozygous crossed with wild type CD1 mice were used in this study.

Plasmid constructs. Plasmids encoding pCAG-SpCas9-VQR-P2A-EGFP, pCAG-SpCas9-VRQR-P2A-EGFP, and pCAG-KKH-SaCas9-P2A-EGFP sequences were generated *via* isothermal assembly. To generate sgRNA plasmids, oligonucleotides were synthesized by Integrated DNA Technologies (Coralville, Iowa, USA), annealed, and ligated into BsmBI digested BPK2660 (Addgene #70709) or BPK1520 (Addgene #65777) for SaCas9 and SpCas9 sgRNAs, respectively.

Subretinal injection. P0-P2 pups were anesthetized by hypothermia and subretinally injected using standard method [25]. Briefly, 0.5µl of DNA solution containing Cas9-encoding plasmid with or without the sgRNA bearing plasmid (absolute amount of DNA is 0.6 µg for Cas9 and 0.3µg for sgRNA, respectively) was injected into the subretinal space using a 34G Hamilton syringe, followed by *in vivo* electroporation using five 90V square pulses of 50 milliseconds duration with a Electro Square Porator (BTX, Holliston, MA).

Retina dissociation and cell sorting. Eye were enucleated and stored in BGJB medium (Thermo Fisher Scientific, Waltham, MA) on ice. Retinas were isolated under a fluorescent dissection microscope to record the transfected region. 3-8 retinas were pooled and dissociated into single cells by incubation in solution A containing 1mg/ml pronase (Sigma-Aldrich, St. Louis, MO) and 2mM EGTA in BGJB medium at 37°C for 20 minutes. Solution A was gently removed from the vial, followed by adding equal amount of solution B containing 100 U/ml DNase I (New England Biolabs, Cambridge, MA), 0.5% BSA, 2mM EGTA in BGJB medium. Cells were spin down at 700rpm for 3 min, supernatant was removed and cells were re-suspended in 1 X phosphate-buffered saline (PBS), filtered through the Cell Strainer (BD Biosciences, San Jose, CA), and submitted for sorting. EGFP positive and negative cells were collected by Cytomation MoFlo Cell Sorter (Cytomation, Fort Collins, CO).

Genomic DNA extraction and PCR. Genomic DNAs extraction from sorted cells was performed using DNA Extraction solution (Epicenter, Madison, WI) following the manufacturer's instructions. PCR using Taq-Pro Red Complete (Denville Scientific, Holliston, MA) and 100ng of

genomic DNAs as template was performed to to amplify the sequence flanking the on-targeting and top 10 predicted off-targeting sequences for tru-sgRNA2 (**Supplementary table 1, 2**). PCR thermocycling was conducted at 94°C for 4 minutes, followed by 35 cycles at 94°C for 30 seconds, 58°C for the P23H on-target primers or 59.4°C for the off-target sites, respectively, for 30 seconds, and 72°C for 30 seconds, followed by a terminal elongation step at 72°C for 10 minutes.

RNA extraction, RT-PCR. Total RNA from sorted EGFP positive and negative cells was extracted using the RNeasy Micro Kit (Qiagen, Hilden, Germany). Total RNA was reverse transcribed with the SuperScript IV First-Strand Synthesis System using Oligo$(dT)_{20}$ primer (Thermo Fisher Scientific, Rockford, IL). cDNA was used for PCR amplification with P23H primers using the condition described above and subjected for NGS analysis.

Targeted deep sequencing. PCR amplicons were analyzed by NGS performed by CCIB DNA core Facility at Massachusetts General Hospital (Cambridge, MA). Partial Illumina adaptor sequences and unique identifiers (barcodes) were attached by ligation to the 5' and 3' ends of the PCR amplicons. A subsequent low-cycle PCR amplification step completed the addition of full-length adaptor sequences. Paired-end sequencing of the resulting TruSeq-compatible paired-end Illumina libraries was performed on the Illumina MiSeq platform, utilizing V2 chemistry. Sequencing data was analyzed using CRISPResso program following by customized algorithm to correct nonsense single nucleotide polymorphisms (SNPs) due to NGS errors and consolidate indel counts [26].

Immunostaining and microscope imaging. Mice were perfused with 4% para-formaldehyde (PFA) in PBS and eyes were marked for orientation using a small vessel cauterizer (Fine Scientific Tools, Foster City, CA) and enucleated. Eyes were post-fixed in 4% PFA for 2-3 hours, transferred into 30% sucrose in PBS at 4°C for overnight. Eye cups were embedded into OCT and 10µM sections were cut using Cryostat (Leica Microsystems). Cryosections were stained with 1: 1000 mouse anti-rhodopsin antibody (MAB5356, EMD Millipore, Billerica, MA), incubated at 4°C for overnight, followed by staining with goat anti mouse Alexa Fluor 555 secondary antibody (A-21422, Thermo Fisher, Waltham, MA) at 1: 1000 dilution for 1 hour at room temperature, and counterstained with Hoechst (62249, Thermo Fisher Scientific) at room temperature for 10 minutes, and mounted with Fluoromout G (Electron Microscopy Sciences, Hatfield, PA). Images were taken using the Eclipse Ti microscope.

Statistical analysis

All data was presented as mean ± s.e.m. Two-tailed unpaired t-test was used for data analysis. Statistical significance was considered when P value is < 0.05, 0.01 or 0.001.

Acknowledgements

This study is supported by Fighting Blindness Foundation (Q.L.); Research to Prevent Blindness Foundation (Q.L.); NIH RO1 EY012910 (E.A.P. and Q.L.); Banting (Natural Sciences and Engineering Research Council of Canada) (B.P.K.); Charles A. King Trust Postdoctoral Fellowships (B.P.K.); NIH R35 GM118158 (B.P.K., M.S.P., and J.K.J.); and Desmond and Ann Heathwood MGH Research Scholar Award (J.K.J.).

Author contributions statement

P.L., B.P.K., and Q.L. contributed to experimental design; B.P.K. and Q.L. designed the Cas9 and sgRNAs constructs; P.L., B.P.K. and M.S.P. performed the production of plasmid constructs; P.L. and Q.L. designed and performed *in vivo* experiments with technical help from M.Y.L. and S.H.G.; P.L. and M.Y.L. executed *in vitro* experiments; P.L., D.N., and Q.L. analyzed the deep sequencing data; P.L. and Q.L. performed *in vivo and in vitro* data analysis; E.A.P, J.K.J, and Q.L. contributed to study conception and interpretation; P.L. and Q.L. drafted the manuscript; B.P.K., S.H.G., E.A.P., J.K.J. and Q.L. revised the manuscript. Q.L. supervised the overall project, and performed the final manuscript preparation. All authors discussed the results, assisted in the preparation of the manuscript and approved the final version.

References

1. Nienhuis, A.W., Nathwani, A.C. & Davidoff, A.M. Gene Therapy for Hemophilia. *Mol Ther* **25**, 1163-1167 (2017).
2. Chacon-Camacho, O.F. & Zenteno, J.C. Gene therapy for vision restoration in patients with Leber congenital amaurosis (LCA) due to RPE65 gene mutations: beginning the phase IV trial. *Gac Med Mex* **153**, 276-278 (2017).
3. Nguyen, A.T., Campbell, M., Kiang, A.S., Humphries, M.M. & Humphries, P. Current therapeutic strategies for P23H RHO-linked RP. *Adv Exp Med Biol* **801**, 471-476 (2014).
4. Hsu, P.D., Lander, E.S. & Zhang, F. Development and applications of CRISPR-Cas9 for genome engineering. *Cell* **157**, 1262-1278 (2014).
5. Courtney, D.G.*, et al.* CRISPR/Cas9 DNA cleavage at SNP-derived PAM enables both in vitro and in vivo KRT12 mutation-specific targeting. *Gene Ther* **23**, 108-112 (2016).
6. Shin, J.W.*, et al.* Permanent inactivation of Huntington's disease mutation by personalized allele-specific CRISPR/Cas9. *Hum Mol Genet* **25**, 4566-4576 (2016).
7. Malkki, H. Huntington disease: Selective deactivation of Huntington disease mutant allele by CRISPR-Cas9 gene editing. *Nat Rev Neurol* **12**, 614-615 (2016).
8. Tsai, S.Q. & Joung, J.K. Defining and improving the genome-wide specificities of CRISPR-Cas9 nucleases. *Nat Rev Genet* **17**, 300-312 (2016).
9. Hsu, P.D.*, et al.* DNA targeting specificity of RNA-guided Cas9 nucleases. *Nat Biotechnol* **31**, 827-832 (2013).
10. Fu, Y.*, et al.* High-frequency off-target mutagenesis induced by CRISPR-Cas nucleases in human cells. *Nat Biotechnol* **31**, 822-826 (2013).

11. Smith, C.*, et al.* Efficient and allele-specific genome editing of disease loci in human iPSCs. *Mol Ther* **23**, 570-577 (2015).
12. Yamamoto, Y.*, et al.* Allele-specific ablation rescues electrophysiological abnormalities in a human iPS cell model of long-QT syndrome with a CALM2 mutation. *Hum Mol Genet* **26**, 1670-1677 (2017).
13. Yoshimi, K., Kaneko, T., Voigt, B. & Mashimo, T. Allele-specific genome editing and correction of disease-associated phenotypes in rats using the CRISPR-Cas platform. *Nat Commun* **5**, 4240 (2014).
14. Slaymaker, I.M.*, et al.* Rationally engineered Cas9 nucleases with improved specificity. *Science* **351**, 84-88 (2016).
15. Kleinstiver, B.P.*, et al.* High-fidelity CRISPR-Cas9 nucleases with no detectable genome-wide off-target effects. *Nature* **529**, 490-495 (2016).
16. Sakami, S.*, et al.* Probing mechanisms of photoreceptor degeneration in a new mouse model of the common form of autosomal dominant retinitis pigmentosa due to P23H opsin mutations. *J Biol Chem* **286**, 10551-10567 (2011).
17. Hartong, D.T., Berson, E.L. & Dryja, T.P. Retinitis pigmentosa. *Lancet* **368**, 1795-1809 (2006).
18. Kleinstiver, B.P.*, et al.* Engineered CRISPR-Cas9 nucleases with altered PAM specificities. *Nature* **523**, 481-485 (2015).
19. Kleinstiver, B.P.*, et al.* Broadening the targeting range of Staphylococcus aureus CRISPR-Cas9 by modifying PAM recognition. *Nat Biotechnol* **33**, 1293-1298 (2015).
20. Fu, Y., Sander, J.D., Reyon, D., Cascio, V.M. & Joung, J.K. Improving CRISPR-Cas nuclease specificity using truncated guide RNAs. *Nat Biotechnol* **32**, 279-284 (2014).
21. Stemmer, M., Thumberger, T., Del Sol Keyer, M., Wittbrodt, J. & Mateo, J.L. CCTop: An Intuitive, Flexible and Reliable CRISPR/Cas9 Target Prediction Tool. *PLoS One* **10**, e0124633 (2015).
22. van Overbeek, M.*, et al.* DNA Repair Profiling Reveals Nonrandom Outcomes at Cas9-Mediated Breaks. *Mol Cell* **63**, 633-646 (2016).
23. Bakondi, B.*, et al.* In Vivo CRISPR/Cas9 Gene Editing Corrects Retinal Dystrophy in the S334ter-3 Rat Model of Autosomal Dominant Retinitis Pigmentosa. *Mol Ther* **24**, 556-563 (2016).
24. Latella, M.C.*, et al.* In vivo Editing of the Human Mutant Rhodopsin Gene by Electroporation of Plasmid-based CRISPR/Cas9 in the Mouse Retina. *Mol Ther Nucleic Acids* **5**, e389 (2016).
25. Matsuda, T. & Cepko, C.L. Electroporation and RNA interference in the rodent retina in vivo and in vitro. *Proc Natl Acad Sci U S A* **101**, 16-22 (2004).
26. Pinello, L.*, et al.* Analyzing CRISPR genome-editing experiments with CRISPResso. *Nat Biotechnol* **34**, 695-697 (2016).

Figures.

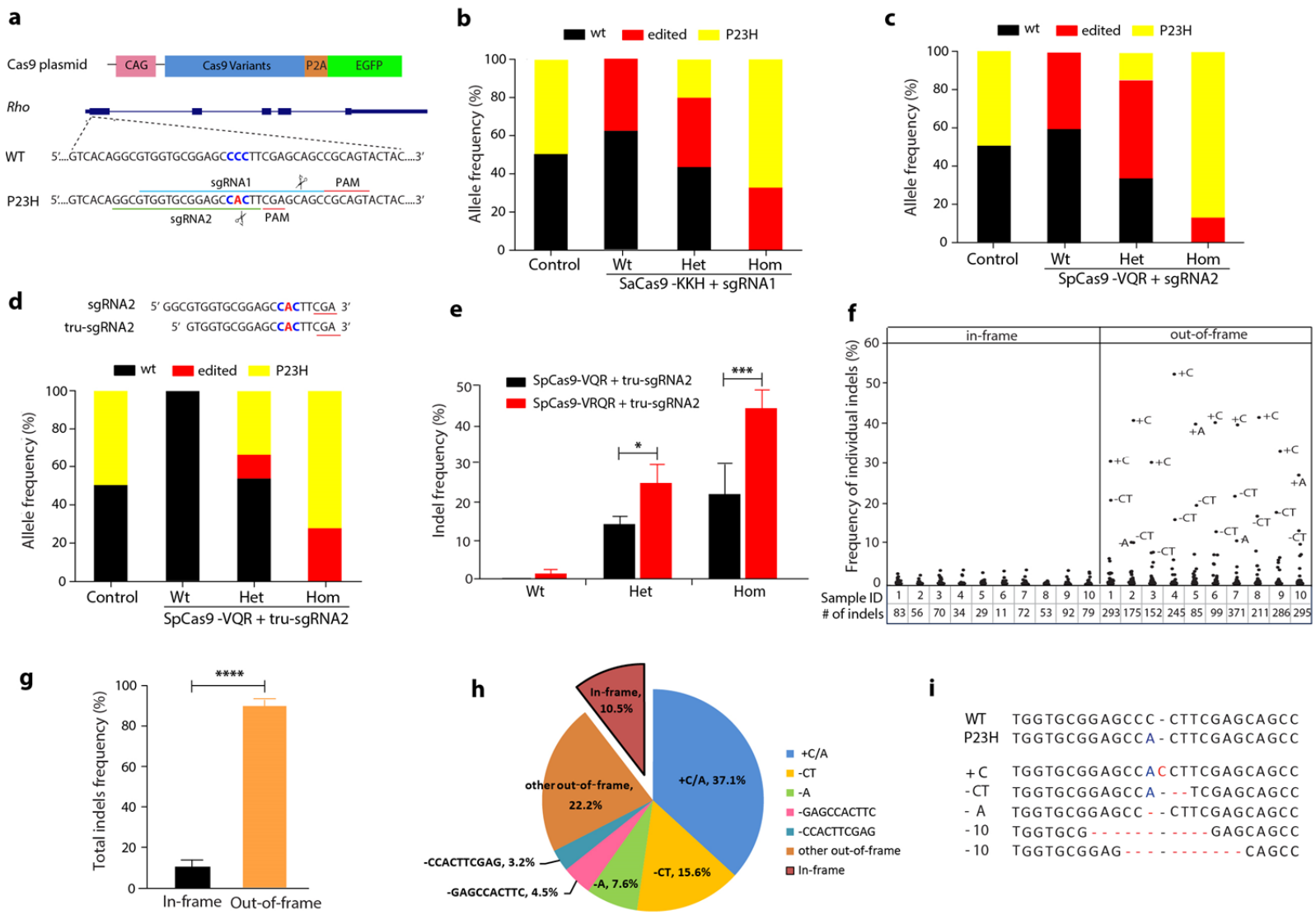
a
Cas9 plasmid
CAG
Cas9 Variants
P2A
EGFP
Rho
WT 5'...GTCACAGGCGTGGTGCGGAGCCCCTTCGAGCAGCCGCAGTACTAC...3'
sgRNA1
PAM
P23H 5'...GTCACAGGCGTGGTGCGGAGCCACTTCGAGCAGCCGCAGTACTAC...3'
sgRNA2
PAM
b
wt
edited
P23H
Allele frequency (%)
Control
Wt
Het
Hom
SaCas9 -KKH + sgRNA1
c
wt
edited
P23H
Allele frequency (%)
Control
Wt
Het
Hom
SpCas9 -VQR + sgRNA2
d
sgRNA2 5' GGCGTGGTGCGGAGCCACTTCGA 3'
tru-sgRNA2 5' GTGGTGCGGAGCCACTTCGA 3'
wt
edited
P23H
Allele frequency (%)
Control
Wt
Het
Hom
SpCas9 -VQR + tru-sgRNA2
e
SpCas9-VQR + tru-sgRNA2
SpCas9-VRQR + tru-sgRNA2
Indel frequency (%)
Wt
Het
Hom
f
in-frame
out-of-frame
Frequency of individual indels (%)
Sample ID
# of indels
g
Total indels frequency (%)
In-frame
Out-of-frame
h
In-frame, 10.5%
other out-of-frame, 22.2%
+C/A, 37.1%
-CT, 15.6%
-A, 7.6%
-GAGCCACTTC, 4.5%
-CCACTTCGAG, 3.2%
+C/A
-CT
-A
-GAGCCACTTC
-CCACTTCGAG
other out-of-frame
In-frame
i
WT TGGTGCGGAGCCC-CTTCGAGCAGCC
P23H TGGTGCGGAGCCA-CTTCGAGCAGCC
+C TGGTGCGGAGCCACCTTCGAGCAGCC
-CT TGGTGCGGAGCCA---TCGAGCAGCC
-A TGGTGCGGAGCC--CTTCGAGCAGCC
-10 TGGTGCG------GAGCAGCC
-10 TGGTGCGGAG-------CAGCC

Figure 1. P23H allele-specific targeting efficiency and indel profile analysis *in vivo*. (**a**) Schematic overview of CRIPSR/Cas9 constructs and their target sites in the *Rho*-P23H allele. Cas9 construct (top panel). **(b-d)** sgRNA screening in injected wt, P23H heterozygous (het) and homozygous (hom) mice. Control: uninjected het mice. Allele frequencies of wt, P23H and edited alleles with indels were determined by the percentage of reads detected in NGS data. **(b)** sgRNA1 with SaCas9-KKH; (**c**) sgRNA2 with SpCas9-VQR. (**d**) Sequences of sgRNA2 and tru-sgRNA2 (top panel). Allele frequencies from retinas injected with SpCas9-VQR + tru-sgRNA2 (bottom). **(e)** Cleavage efficiency of SpCas9-VQR (n=3) vs. SpCas9-VRQR (n=3) combined with tru-sgRNA2 in wt, het and hom mice. **(f)** Distribution and frequency of individual in-frame (right) and out-of-frame (left) indels from P23H het mice injected with SpCas9-VRQR and tru-sgRNA2 in 10 independent experiments. The total number of indel panels for each sample is listed at bottom. (**g**) Average percentage of in-frame vs. out-of-frame indels (n=10). (**h**) Average percentage of top 5 and other out-of-frame and in-frame indels. (**i**) Representative sequences of top five indel patterns. **** $P < 0.0001$, *** $P < 0.001$, * $P < 0.05$.

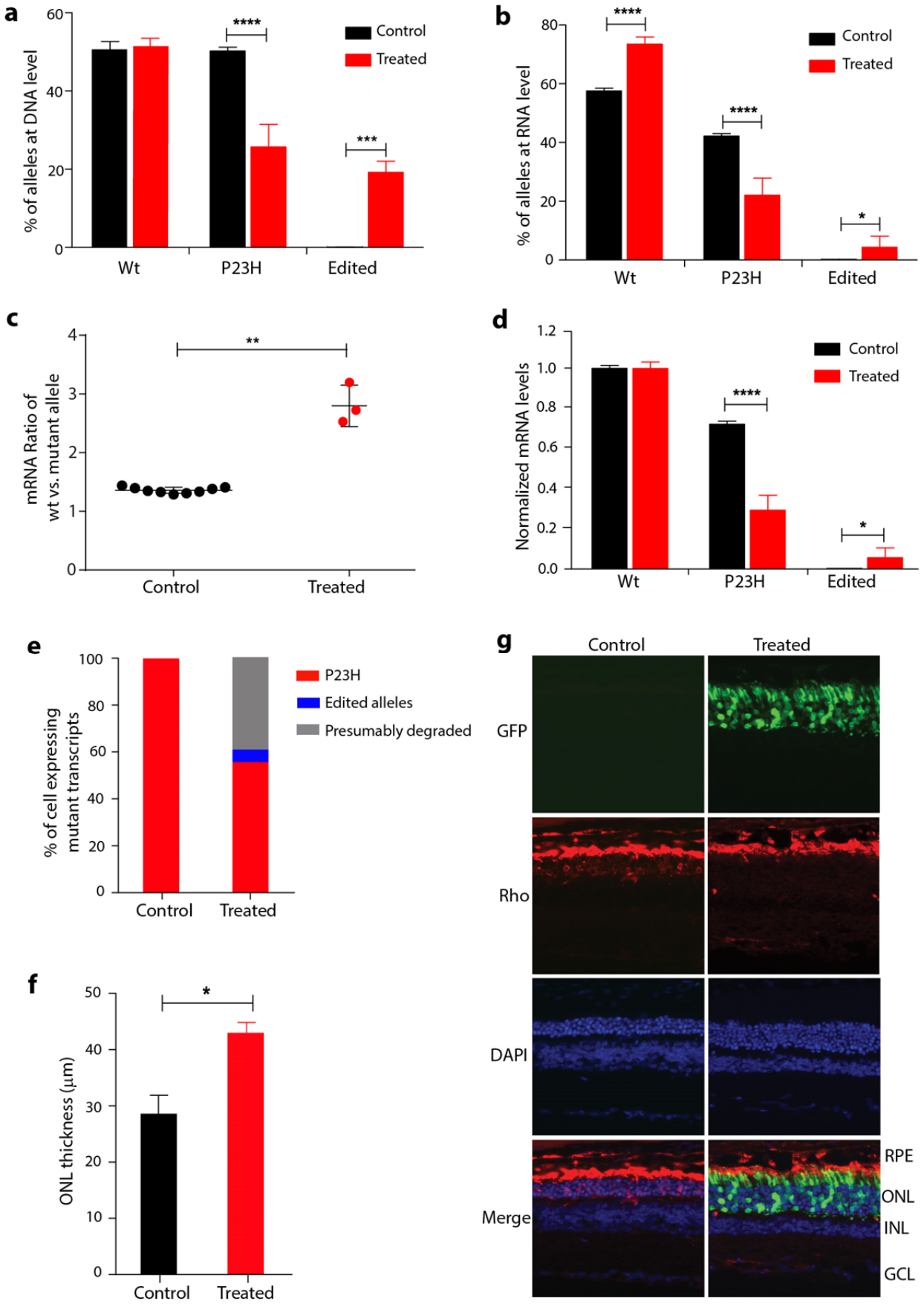
a
% of alleles at DNA level
60
40
20
0
****
***
Control
Treated
Wt
P23H
Edited
b
% of alleles at RNA level
80
60
40
20
0
****
****
*
Control
Treated
Wt
P23H
Edited
c
mRNA Ratio of wt vs. mutant allele
4
3
2
1
0
**
Control
Treated
d
Normalized mRNA levels
1.2
1.0
0.8
0.6
0.4
0.2
0.0
****
*
Control
Treated
Wt
P23H
Edited
e
% of cell expressing mutant transcripts
100
80
60
40
20
0
P23H
Edited alleles
Presumably degraded
Control
Treated
f
ONL thickness (µm)
50
40
30
20
10
0
*
Control
Treated
g
Control
Treated
GFP
Rho
DAPI
Merge
RPE
ONL
INL
GCL

Figure 2. Expression of P23H allele and photoreceptor preservation after gene editing with tru-sgRNA2 and SpCas9-VRQR in P23H heterozygous mice. Relative DNA level **(a)** and RNA level **(b)** of wt, P23H allele and edited allele in the treated retinas (n=3) expressing SpCas9-VRQR and tru-sgRNA2 vs. untreated retinas (n=9) in P23H het mice 14 days post injection. **(c)** The ratio of wt to mutant (P23H + edited) alleles at mRNA level in the treated and untreated retinas. **(d)** Normalized RNA level of wt, P23H, and indel in the treated and untreated retinas. **(e)** Percentage of cells presumably expressing wt/P23H, wt/edited P23H, and wt only in the treated and untreated retinas. **(f)** Comparison of ONL thickness of the treated area to its adjacent untreated central area (n=3). **(g)** Retinal images from the treated region marked by EGFP expression (left) and the adjacent untreated region (right) (top panel) in the P23H het mice at 5 weeks post injection. Rhodopsin expression is detected by rhodopsin antibody (red), the EGFP signal indicates transfection (green), and nuclei were counterstained with Hoechst (blue). RPE: retinal pigment epithelium, ONL: outer nuclear layer, INL: inner nuclear layer. GCL: ganglion cell layer. **** $P < 0.0001$, *** $P < 0.001$, * $P < 0.05$.

Supplementary materials

Supplementary Figure 1. Evaluation of SpCas9-VRQR specificity when paired with tru-sgRNAs ***in vivo***. Off-target editing frequency in P23H het mice was examined at the top 10 off-target sites. Samples were collected and analyzed 7 days post injection. Off-target data is represented as mean ± s.e.m(n=3), NGS of the PCR amplicon of the P23H site is used as positive control and that from the un-injected cells as a negative control.

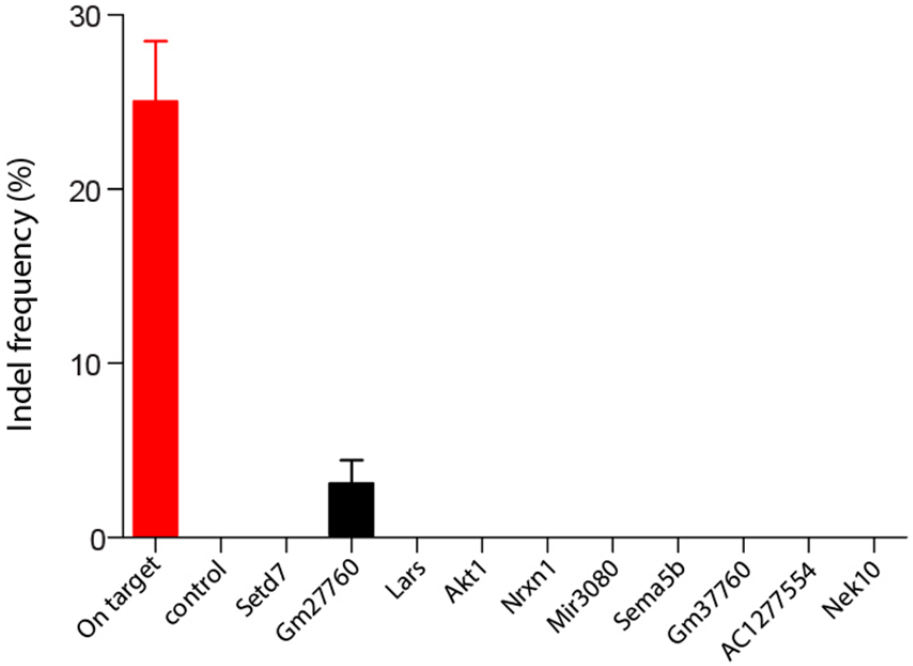

Supplementary Figure 2. indel profiles from 10 separate experiments. Total percentage of edited alleles carrying in-frame (red) or out-of-frame (blue) indels in P23H het mice injected with SpCas9-VRQR and tru-sgRNA2, data was analyzed 7 days post-injection.

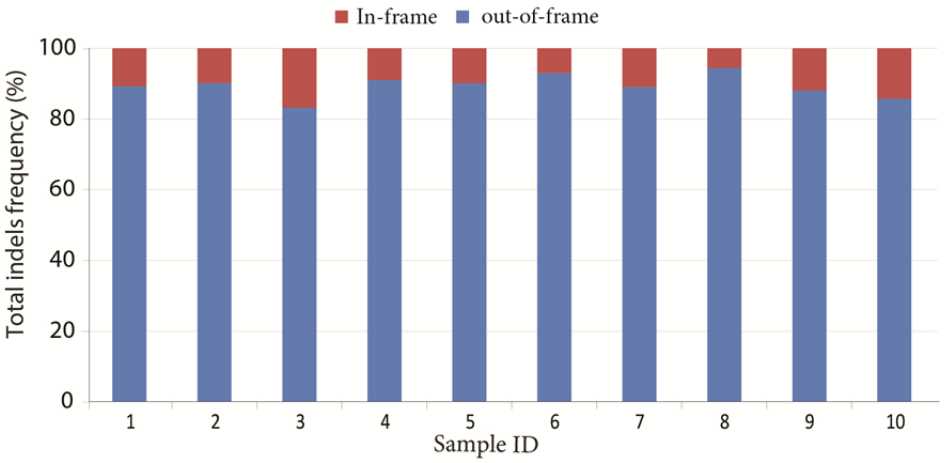

Supplementary Table 1. Top 20 out of 2074 predicted off-target sites of tru-sgRNA2 and SpCas9-VRQR

Coordinates (GRCm38/mm10)	MM*	Target_sequence**	PAM	Position	Gene name
Chr6:115932059-115932078	1	GTGGT[GCGGAGCCCCTT]	CGA	Exonic	Rho
chr3:51534318-51534337	2	GGTGT[GCGGAGCCACTT]	GGA	Intronic	Setd7
chr15:5877846-5877865	1	GTGGT[GTGGAGCCACTT]	TGA	Intergenic	Gm27760
chr18:42216853-42216872	4	ACCCCT[GCGGAGCCACTT]	TGA	Exonic	Lars
chr12:112667982-112668001	2	GTGGG[GCTGAGCCACTT]	GGA	Exonic	Akt1
chr17:90591810-90591829	3	GAGCT[GAGGAGCCACTT]	GGA	Intronic	Nrxn1
chr15:82952543-82952562	4	AAGCC[GCGGAGCCACTT]	TGA	Intergenic	Mir3080
chr16:35528273-35528292	4	CAGTA[GCGGAGCCACTT]	TGA	Intergenic	Sema5b
chr1:91917859-91917878	3	CTTGT[GCAGAGCCACTT]	GGA	Exonic	Gm37600
chr8:121126629-121126648	3	ATGGA[GGGGAGCCACTT]	GGA	Intronic	AC127554.1
chr14:14957653-14957672	2	GTGGT[ACTGAGCCACTT]	GGA	Intronic	Nek10
chr6:28464010-28464029	3	GTTCT[GGGGAGCCACTT]	CGA	Intergenic	Gm43264
chr1:48454326-48454345	3	GTAAT[GAGGAGCCACTT]	TGA	Intergenic	Gm23240
chr7:118779695-118779714	2	GAGGT[GCGGGGCCACTT]	CGA	Exonic	9030624J02Rik
chr12:85072399-85072418	3	TTGGT[TTGGAGCCACTT]	GGA	Intergenic	Ylpm1
chr15:41792995-41793014	4	AGTGT[GAGGAGCCACTT]	TGA	Intronic	Oxr1
chr16:43727298-43727317	4	AAAGT[GGGGAGCCACTT]	TGA	Intergenic	Drd3
chr19:38652109-38652128	3	GAGGT[AAGGAGCCACTT]	GGA	Exonic	Plce1
chr10:114571848-114571867	3	GAGGT[TGGGAGCCACTT]	GGA	Intronic	Trhde
chr4:22491277-22491296	4	CAGTT[GGGGAGCCACTT]	CGA	Intronic	RP23-381K3.5
chr4:100378125-100378144	3	GTAGA[GCAGAGCCACTT]	TGA	Intronic	Gm12706

* *In silico* predicted off-target sites with 1-5 mismatches (MM) by CCTop-CRISPR/Cas9 target online predictor using input sequence GTGGTGCGGAGCC**A**CTTCGA and NGA PAM sequence.
**The sequences in the brackets are the seed sequence; nucleotides in red indicate mismatched positions.

Supplementary Table 2. Primer sets and the size of PCR product used in this study.

Gene Name	Forward Primer	Reverse Primer	size (bp)
Rho-P23H	5' CGAGAGCCGCAGCCATGAAC 3'	5' CCCAGCACGATGAGCAGGAAC 3'	166
Setd7	5' GGCAGAGGAATACAAGGGATAG 3'	5' ACGTGTGGTCCAGGTTAAAG 3'	200
Gm27760	5' CAGAATTCAGCCCAGATCCTT 3'	5' GTCAGGAGAACTTCAGTCTTGG 3'	205
Lars	5' AAAGGCCACCTGTCTGTTCC 3'	5' GACTGACAAGCAGCCAGCTC 3'	200
Akt1	5' GTTCTGGCCATCCACACA 3'	5' AGTCCTCTCGGCTTCCT 3'	215
Nrxn1	5' CTTTCATTTGGTTCATAAGAACAGC 3'	5' CTCACTGTGTAGAGAGGAAATCA 3'	276
Mir3080	5' CTGTCAACCTGAACTAATCAAACC 3'	5' GCCACCTAAGCTCAGTTTCT 3'	246
Sema5b	5' AATGGTTGAATTCCAGCAACAG 3'	5' GCTCCCTGTGAAATGAAGACTA 3'	258
Gm37760	5' GTTGTGGTCAGTTGGTCATTAG 3'	5' GGCTCTATGTCCCTATTCTGAG 3'	225
AC1277554	5' CACAGTTTCCACTTGCTTTC 3'	5' GCATTTGTAAAGCCTGCAT 3'	266
Nek10	5' GGAAGAGAAAGGCACTCACA 3'	5' CTTAACATCCTTCAGCACCCTA 3'	210